Shape Memory Behavior of FeNiCoTi Single and Polycrystals

HUSEYIN SEHITOGLU, X.Y. ZHANG, T. KOTIL, D. CANADINC, Y. CHUMLYAKOV, and H.J. MAIER

We present experimental and theoretical evidence of thermoelastic martensites in Fe29Ni18Co4Ti alloys. In this class of alloys, the high strength in the austenite domains limits the slip deformation as verified with transmission electron microscopy. The restriction of slip permits a higher degree of recoverability of the transformation. Using both single crystals with [123] orientation and polycrystals, the appearance of martensite plates upon deformation, and their reversion back to austenite upon heating (the shape memory effect), is revealed with *in-situ* optical microscopy. Theoretical results for the transformation strains and the detwinning of martensite are presented, which demonstrate convincingly the potential of these classes of alloys. Electrical resistance measurements identified the stress and temperature levels at the onset of forward and reverse transformations in isothermal deformation and thermal cycling experiments, respectively. The return of the electrical resistance to its reference value, upon austenite to martensite followed by martensite to austenite transformation, verified the recovery in the transformation strains measured in the experiments.

I. INTRODUCTION

IT is well known that a number of Ni- and Cu-based materials display shape memory behavior and also pseudoelastic response.[1,2,3] The shape memory behavior is defined as the recoverability of deformation upon heating above a critical temperature. The pseudoelastic response refers to the forward transformation upon loading and reverse transformation upon unloading under isothermal conditions. The shape memory behavior has been observed in other materials such as certain iron alloys but the research in iron-based alloys lagged its Ni- and Cu-based counterparts. Previously, the primary focus has been on FeMnSi alloys,[4] where the reversibility of the transformation has been curtailed by the underlying slip deformation. In the present work, we study FeNiCoTi alloys, which are a new class of materials exhibiting thermoelastic martensite, hence, reversible transformations from austenite to martensite. The transformation can be induced *via* a change in temperature or the application of stress at temperatures exceeding the martensite start temperature, M_s. Three major groups of researchers have studied these classes of alloys. The group of Kokorin *et al.*[5] in the Ukraine has considered Co-rich (>20 wt pct) compositions to reduce the tetragonality ratio and minimize the volume change upon deformation. They demonstrated recoverable strains of less than 0.5 pct in temperature cycling experiments in early work.[6] In more recent work,[7] they have demonstrated recoverable strains near 0.7 pct. In addition to the length change measurements, they noted the changes in magnetic transition from ferromagnetic to paramagnetic states upon transformation from austenite to martensite. The second group who conducted extensive work on FeNiCoTi alloys was Hornbogen and colleagues[8,9] in Germany. They have considered compositions with lower Co (<20 pct) and higher Ni (>20 pct) contents compared to Kokorin. Their main emphasis has also been to optimize aging treatments and to strengthen the austenite phase with the introduction of fine precipitates. Finally, Maki[10] in Japan has made the observation that thin martensites are responsible for the reversible transformations. We note that these previous treatments have not considered theoretical calculations of transformation strain levels and also reported transformation strain levels below 0.7 pct in all cases. Building on our previous study,[11] in this article, we provide experimental results that clearly demonstrate transformation strain levels near 2 pct in tension. We also provide theoretical results that confirm the high transformation strain potential in these materials.

The transformation strains depend on the crystal orientation and the loading direction. Theoretical calculations have been carried out to predict the twin types and the associated habit planes.[11] In early work,[11] we have demonstrated theoretically that these classes of alloys have the potential to possess transformation strains in excess of 10 pct. In the present work, we extend the results to include the contribution from detwinning strains.

Combined with their high strength and relatively lower cost compared to the well-known NiTi alloys, the FeNiCoTi alloys can be used in various structural applications. The aging treatment is typically held at temperatures in the range 550 °C to 700 °C[5–9] in FeNiCoTi alloys and the aging increases the strength of austenite upon precipitation and also by reducing the tetragonality of the martensite. Both these factors contribute to improvement in shape memory properties. In our present work, we have measured the strength levels upon several different heat treatments and discovered that aging at 600 °C for 85 minutes provided the highest strength and hardening (hence, slip resistance). We then proceed with tension and compression experiments first, followed by temperature cycling experiments under constant stress. We have also measured the changes in resistance

HUSEYIN SEHITOGLU, Grayce Wicall Gauthier Professor, X.Y. ZHANG, Visiting Scholar, T. KOTIL, Visiting Scholar, on sabbatical leave from the Aeronautical and Astronautical Engineering Department, Istanbul Technical University, Istanbul, Turkey, and D. CANADINC, Research Assistant, are with the Department of Mechanical and Industrial Engineering, University of Illinois, Urbana, IL 61801. Contact e-mail: huseyin@uiuc.edu Y. CHUMLYAKOV, Professor, is with the Siberian Physical-Technical Institute, Tomsk, 6340502, Russia. H.J. MAIER, Professor, is with Lehrstühl fur Werkstoffkunde, University of Paderborn, 33095 Paderborn, Germany.

Manuscript submitted May 15, 2002.

during deformation and also under temperature cycling conditions. This type of measurement provided a unique insight into the onset of transformation to martensite (martensite start and finish temperatures) and transformation to austenite (austenite start and finish temperatures).

II. MATERIAL AND MICROSTRUCTURE

Ingots were originally cast by Specialty Metals with Fe-29Ni-18Co-4Ti (wt pct) composition in an inert environment. The first portion of the ingots was then remelted and grown to single crystals using the Bridgman method. After single-crystal growth homogenization of the samples was undertaken at 1080 °C for 24 hours followed by water quench. The specimens were aged at 600 °C for 85 minutes to produce a fine precipitate structure. During aging, coherent ordered particles ($L1_2$ - Ni_3Ti precipitates) form, strengthening the matrix. A second portion of the ingots was subjected to consecutive hot rolling (900 °C) and cold rolling treatments at room temperature. The resultant material after cold rolling had a 6.8 × 6.8-mm cross section. The cold-rolled material was subjected to a 1150 °C, 10 minute recrystallization followed by the 600 °C, 85 minute heat treatment to produce a polycrystalline microstructure. Differential scanning calorimetry was performed on aged polycrystals using the Perkin-Elmer Pyris 1 DSC system. The following transformation temperatures were observed: $M_s = -85$ °C, $A_s = -20$ °C, and $A_f = 71$ °C. The martensite finish temperature could not be detected from the DSC curves, but is near −120 °C, based on the strain-temperature response of polycrystalline samples, to be reported later.

Transmission electron microscopy studies were undertaken on both the single-crystal and polycrystalline samples. The results are summarized in Figures 1(a) through (f). In Figure 1(a), we note the presence of fine martensites. Interface dislocations are noted in Figure 1(b) as well as ultrafine precipitates within the martensite domain. Figures 1(c) through (d) represent low dislocation density, planar structures in the austenitic domains. It is noted that dislocations form pileups and the dislocation structure implies that dislocations cut the precipitates rather than bypass them. In both Figures 1(d) and (e), a fine martensite platelet is visible. Finally, we note the presence of mechanical twinning in Figure 1(f). A single twin system is activated in the case of [123] crystals with multiple systems present for the polycrystalline case.

For resistance measurements, a four-point technique was used with a resistance resolution of $\pm 1\ \mu\Omega$. Tinsley senator thermometer bridge (model 5840D), operating with alternating current, provided true measurements of resistance with currents approximately 1 mA. The effect of specimen geometry changes and the temperature dependence of resistivity have been compensated to provide a true measure of change in resistivity due to transformation. This correction is performed as follows:

$$\left[\frac{\Delta R}{R_0}\right]_{\text{trans}} = \left[\frac{\Delta \rho}{\rho_0}\right]_{\text{meas}} - (1 + 2\nu)\,\varepsilon - c(T)(T - T_0)$$

In this equation, the measured change in resistivity is denoted as $\left[\frac{\Delta \rho}{\rho_0}\right]_{\text{meas}}$ and the transformation-induced resistivity change is given as $\left[\frac{\Delta R}{R_0}\right]_{\text{trans}}$. The applied strain is denoted as ε, and ν is the Poisson's ratio. The $c(T)$ is a temperature coefficient, that accounts for the change in resistivity with temperature in the absence of transformation or strain. The $c(T)$ can be described as a constant as a first approximation. For the polycrystalline austenite phase, the value of the temperature coefficient, $c(T)$, is 2.46 10^{-3} 1/°C.

III. MODELING OF TRANSFORMATION STRAINS AND DETWINNING STRAINS IN TENSION AND COMPRESSION

The martensitic transformation in Fe-SMAs occurs *via* phase change from cubic (austenite) to tetragonal (martensite) lattice. The lattice parameters for the FeNiCoTi alloys have been extensively examined by Kokorin.[13] and for Ni-rich compositions, the lattice constants are approximately described by $a_0 = 3.61$ Å, $a = b = 2.80$ Å, and $c = 3.01$ Å. The lattice constants and the face-centered cubic (fcc) to body-centered tetragonal (bct) transformation can be best visualized with the aid of Figure 2(a). The *x*, *y*, and *z* axes are in the austenite (fcc) coordinate frame and the *X*, *Y*, and *Z* crystal axes represent the bct martensite frame. The bct martensite unit cell is shown within the two fcc cells in the upper figure. The basic martensite lattice undergoes dimensional changes, as shown in Figure 2(a).

In Figure 2(b), we demonstrate schematically the austenite (the framed volume), the twinned martensite (the volume after shape change with internal twins), and the detwinned martensite (volume shown on the right-hand side after detwinning shear). The individual atomic movements are noted during the detwinning process. First, we note the definition of the correspondent variant pair (CVP). The CVP includes two twin-related martensite variants. One of the twin variants has a volume fraction *f* and the other $1 - f$. The detwinning process is the growth (or migration of twin boundaries) of one of the variants (shown in Figure 2(b)) at the expense of the other variant, producing a single variant (single crystal) of martensite. At the end of the detwinning process, the twinned martensitic structure disappears. The vector **n** is the twinning plane normal, **a** is the twinning shear direction, **m** is the habit plane normal, and **b** is the shear of the martensite.

By using energy minimization theory,[12] it was possible to establish the habit plane, transformation direction, and the twin parameters for FeNiCoTi alloy. The transformation vectors are calculated using a procedure outlined for NiTi in Reference 2. We note, however, that in fcc to bct transformation there are three variants. The symmetric portion of the deformation gradients are designated as

$$\mathbf{U}_1 = \begin{bmatrix} \eta_1 & 0 & 0 \\ 0 & \eta_1 & 0 \\ 0 & 0 & \eta_2 \end{bmatrix}, \quad \mathbf{U}_2 = \begin{bmatrix} \eta_2 & 0 & 0 \\ 0 & \eta_1 & 0 \\ 0 & 0 & \eta_1 \end{bmatrix}, \quad \mathbf{U}_3 = \begin{bmatrix} \eta_1 & 0 & 0 \\ 0 & \eta_2 & 0 \\ 0 & 0 & \eta_1 \end{bmatrix} \qquad [1]$$

where $\eta_1 = \frac{\sqrt{2}a}{a_0}$, $\eta_2 = \frac{c}{a_0}$, where a_0 is the lattice parameter

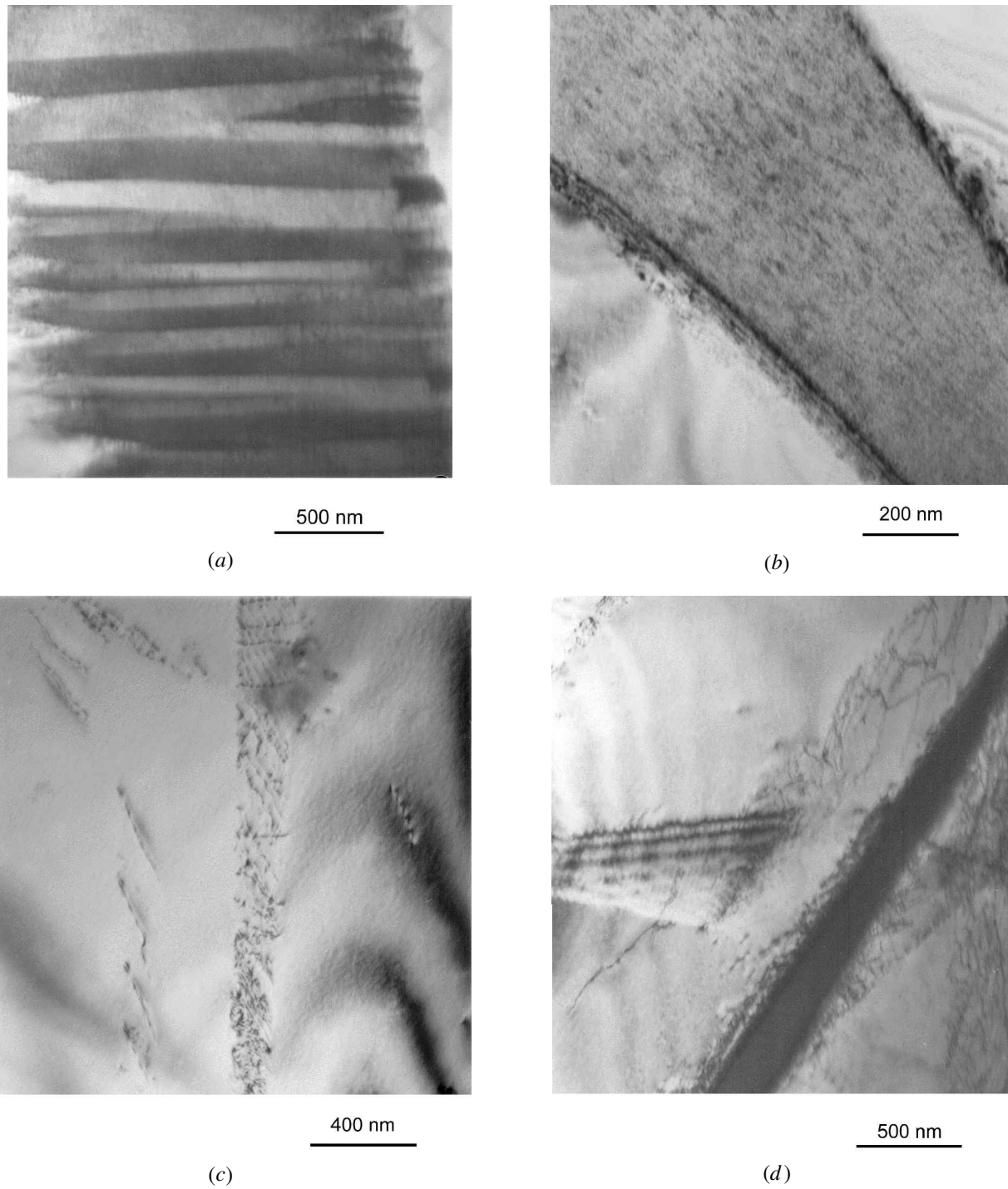

Fig. 1—(*a*) TEM results demonstrating ultrafine martensite variants for the Fe-29 pct Ni-18 pct Co-4 pct Ti polycrystalline specimen subjected to tensile deformation. (*b*) TEM results demonstrating the fine precipitates within the martensitic lamellae for the Fe-29Ni-18Co-4Ti, [123] orientation deformed under tension. Based on orientation of the features with respect to the incoming electron beam, the precipitates within the austenite are not visible. (*c*) TEM results on the FeNiCoTi polycrystalline samples deformed under tension showing low dislocation density in the austenitic domains after the deformation. (*d*) martensite and interface dislocations obtained from the FeNiCoTi polycrystalline samples deformed under tension experiment. (*e*) Martensite variant, interface dislocations at the austenite/martensite interface, and planar slip structures in the austenite domains in polycrystalline deformation experiment, (*f*) evidence of mechanical twinning in the austenite domains in [123] compression deformation experiment.

of austenite and a and c are the lattice parameters of martensite.

The gradient matrix $\mathbf{F}_1$ can be polar decomposed as

$$\mathbf{F}_1 = \mathbf{R}_1 \cdot \mathbf{U}_1 \qquad [2]$$

where $\mathbf{R}_1$ represents a rigid body rotation satisfying $\mathbf{R}_1^T \cdot \mathbf{R}_1 = \mathbf{I}$ ($\mathbf{I}$ is the second rank identity matrix) and $\mathbf{U}_1$ is the symmetric part of $\mathbf{F}_1 \cdot \mathbf{U}_1$ and $\mathbf{R}_1$ can be obtained by

$$\mathbf{U}_1 = \sqrt{\mathbf{F}_1^T \cdot \mathbf{F}_1},\ \mathbf{R}_1 = \mathbf{F}_1 \cdot \mathbf{U}_1^{-1} \qquad [3]$$

where $\mathbf{F}_1^T$ is the transpose of $\mathbf{F}_1$, and $\mathbf{U}_1^{-1}$ is the inverse of $\mathbf{U}_1$.

Any two of the three lattice correspondence variants can

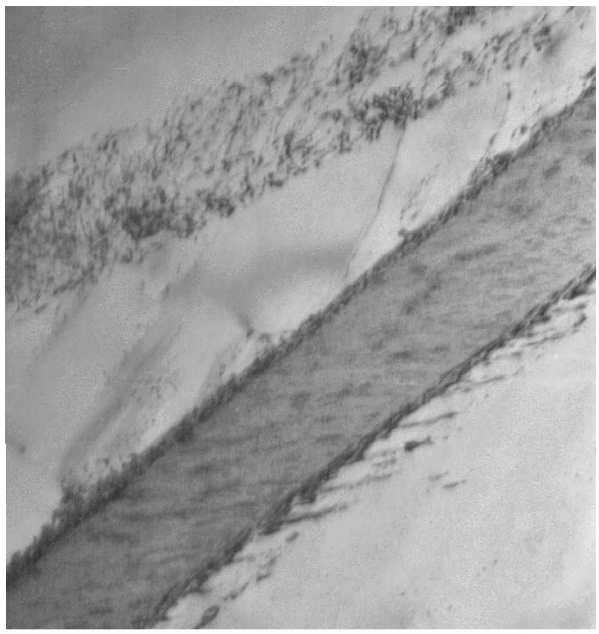

(*e*)

(*f*)

Fig. 1—Continued. (*a*) TEM results demonstrating ultrafine martensite variants for the Fe-29 pct Ni-18 pct Co-4 pct Ti polycrystalline specimen subjected to tensile deformation. (*b*) TEM results demonstrating the fine precipitates within the martensitic lamellae for the Fe-29Ni-18Co-4Ti, [123] orientation deformed under tension. Based on orientation of the features with respect to the incoming electron beam, the precipitates within the austenite are not visible. (*c*) TEM results on the FeNiCoTi polycrystalline samples deformed under tension showing low dislocation density in the austenitic domains after the deformation. (*d*) martensite and interface dislocations obtained from the FeNiCoTi polycrystalline samples deformed under tension experiment. (*e*) Martensite variant, interface dislocations at the austenite/martensite interface, and planar slip structures in the austenite domains in polycrystalline deformation experiment, (*f*) evidence of mechanical twinning in the austenite domains in [123] compression deformation experiment.

form twins. The kinematic compatibility between the two correspondence variants in the twin across the twin plane requires

$$\mathbf{R}_{ij}\mathbf{U}_j - \mathbf{U}_i = \mathbf{a} \quad \mathbf{n} \qquad [5]$$

where $\mathbf{U}_i$ and $\mathbf{U}_j$ are two lattice correspondence variants, which form the twin. The $\mathbf{R}_{ij}$ represents an orthogonal tensor satisfying $\mathbf{R}_{ij}^T \cdot \mathbf{R}_{ij} = \mathbf{I}$; it represents the relative rotation between the two variants. The vector $\mathbf{n}$ is the twinning plane normal, and $\mathbf{a}$ is the twinning shear direction. The subscripts i and j in Eq. [5] represent different choices of the integers {1, 2, 3} and there is no summation of the indices. Six possible pairs of $\mathbf{U}_i$ and $\mathbf{U}_j$ can be formed from the three lattice correspondence variants; therefore, Eq. [5] represents six equations. The unknowns in Eq. [5] are $\mathbf{a}$, $\mathbf{n}$, and $\mathbf{R}_{ij}$ for a given pair of $\mathbf{U}_i$ and $\mathbf{U}_j$. These values can be obtained as follows.

Equation [5] is postmultiplied by $\mathbf{U}_i^{-1}$:

$$\mathbf{R}_{ij}\mathbf{U}_j\mathbf{U}_i^{-1} = \mathbf{I} + \mathbf{a} \quad (\mathbf{n}\mathbf{U}_i^{-}) \text{ (no summation)} \qquad [6]$$

A symmetric matrix $\mathbf{C}$ is formed as

$$\mathbf{C} = (\mathbf{R}_{ij}\mathbf{U}_j\mathbf{U}_i^{-1})^T \cdot (\mathbf{R}_{ij}\mathbf{U}_j\mathbf{U}_i^{-1}) = \mathbf{U}_i^{-1} \cdot \mathbf{U}_j^2 \cdot \mathbf{U}_i^{-1} \qquad [7]$$

where the superscripts T and 2, respectively, represent the transposition and square of a tensor. There are also six different $\mathbf{C}$ values corresponding to the six pairs of $\mathbf{U}_i$ and $\mathbf{U}_j$. The sufficient and necessary condition of Eq. [5] having solutions is that $\mathbf{C}$ has ordered eigenvalues of $\lambda_1 \le \lambda_2 = 1 \le \lambda_3$. Under this case, $\mathbf{C}$ can be written as

$$\mathbf{C} = (\mathbf{I} + \mathbf{n}' \quad \mathbf{a}') \cdot (\mathbf{I} + \mathbf{a}' \quad \mathbf{n}') \qquad [8]$$

where

$$\mathbf{a}' = \mathbf{a},\ \mathbf{n}' = \mathbf{U}_i^{-1} \cdot \mathbf{n} \qquad [9]$$

The vectors $\mathbf{a}'$ and $\mathbf{n}'$ are solved as (Ball and James[12])

$$\mathbf{a}' = \rho\left(\sqrt{\frac{\lambda_3(\lambda_2 - \lambda_1)}{\lambda_3 - \lambda_1}}\mathbf{e}_1 + \kappa\sqrt{\frac{\lambda_1(\lambda_3 - \lambda_2)}{\lambda_3 - \lambda_1}}\mathbf{e}_3\right) \qquad [10]$$

$$\mathbf{n}' = \rho^{-1}\left(\frac{\sqrt{\lambda_3} - \sqrt{\lambda_1}}{\sqrt{\lambda_3 - \lambda_1}}\right)\left(-\sqrt{\lambda_2 - \lambda_1}\mathbf{e}_1 + \kappa\sqrt{\lambda_3 - \lambda_2}\mathbf{e}_3\right) \qquad [11]$$

where $\mathbf{e}_1$, $\mathbf{e}_2$, and $\mathbf{e}_3$ are the three eigenvectors of matrix $\mathbf{C}$ corresponding to λ_1, λ_2, λ_3, respectively. The constant ρ represents an invariant scaling of the solution and will be used to choose the unit normal vector $\mathbf{n}$. The constant κ can take the value ± 1. We denote the solution of ($\mathbf{a}$, $\mathbf{n}$) with $\kappa = +1$ as ($\mathbf{R}_{ij}^+$, $\mathbf{a}^+$, $\mathbf{n}^+$) and $\kappa = -1$ as ($\mathbf{R}_{ij}^-$, $\mathbf{a}^-$, $\mathbf{n}^-$). The relationships between the twinning elements and $\mathbf{a}$ and $\mathbf{n}$ in the parent phase basis are, respectively,

$$(\mathbf{K}_1^+,\ \eta_1^+,\ \mathbf{K}_2^+,\ \eta_2^+) \| (\mathbf{n}^+,\ \mathbf{U}_i^{-1}\mathbf{a}^+,\ \mathbf{n}^-,\ \mathbf{U}_i^{-1}\mathbf{a}^-) \qquad [12]$$

and

$$(\mathbf{K}_1^-,\ \eta_1^-,\ \mathbf{K}_2^-,\ \eta_2^-) \| (\mathbf{n}^-,\ \mathbf{U}_i^{-1}\mathbf{a}^-,\ \mathbf{n}^+,\ \mathbf{U}_i^{-1}\mathbf{a}^+) \qquad [13]$$

where $\mathbf{K}_1$ is the normal of the first undistorted plane in the twin (usually referred to as the twinning plane); $\mathbf{K}_2$ is the

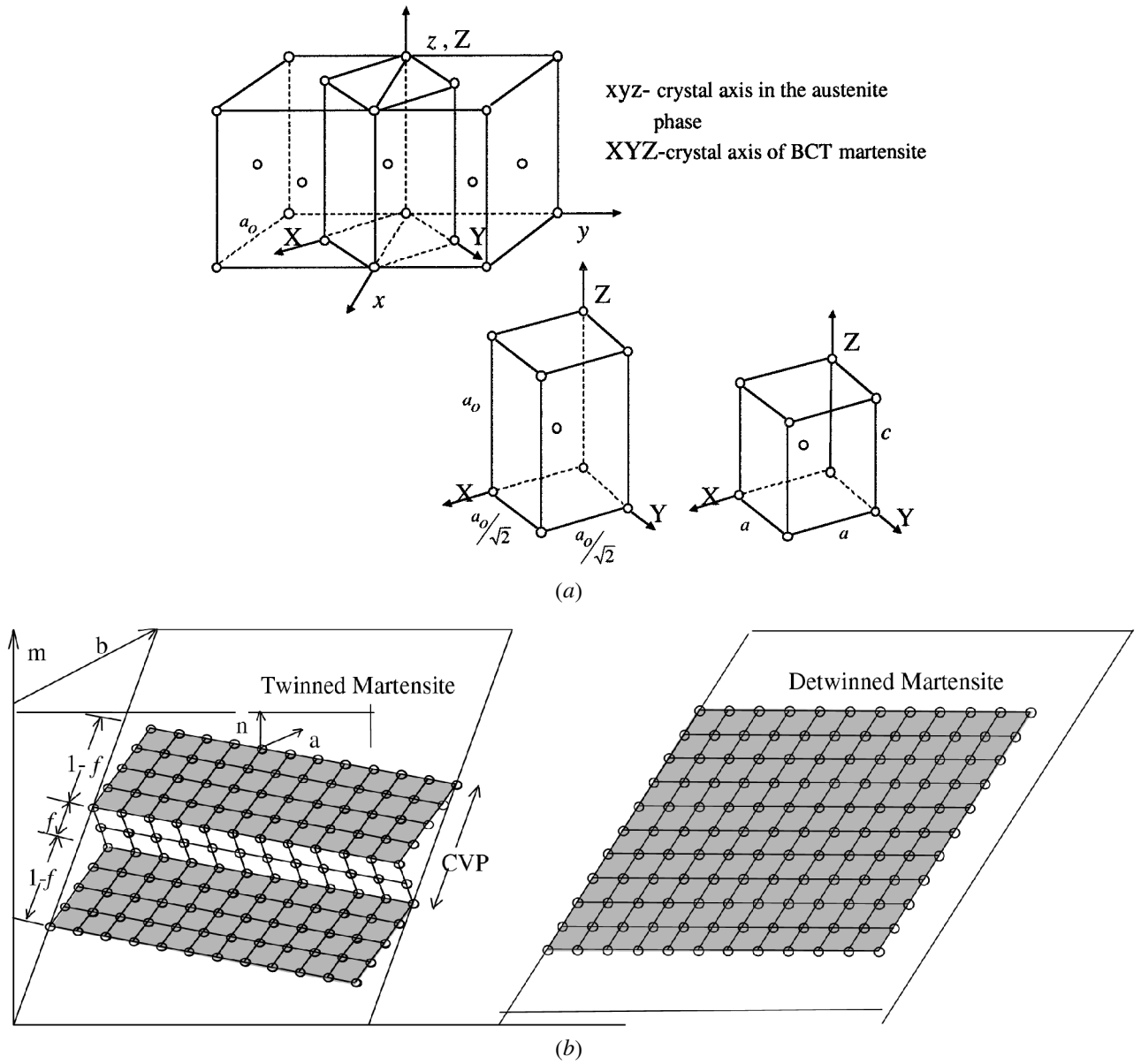

Fig. 2—(*a*) The fcc to bct (tetragonal) phase transformation and lattice constants. The bct lattice is shown inside the fcc lattice in the upper figure. The lattice deformation produces the final bct crystal shown on the right. (*b*) The transformation parameters and the schematic description of the detwinning process.

normal of the second undistorted plane (or conjugate twinning plane), η_1 is the shear direction, which lies in the detwinning plane; and η_2 another undistorted direction in the $\mathbf{K}_2$ plane.

For the cubic to tetragonal transformation, all six equations have solutions and three of the solutions are independent since the pair ($\mathbf{U}_i$, $\mathbf{U}_j$) is equivalent to ($\mathbf{U}_j$, $\mathbf{U}_i$). According to the relationships of [12] and [13], all three variant pairs form compound twins. Each pair can then form two different types of twins (because of $\kappa = \pm 1$), so there are totally six possible twins.

In the work discussed previously, we have determined all the possible twins (number of twins, twin plane normal **n**, and twinning shear vector **a**) by using the invariant plane condition of the twinning plane. The habit plane normals and the transformation strains can then be determined by using the invariant plane conditions across the habit plane, which requires

$$\mathbf{F}_M - \mathbf{I} = \mathbf{b} \quad \mathbf{m} \qquad [14]$$

where $\mathbf{I}$ is the identity tensor, $\mathbf{m}$ is the habit plane normal, $\mathbf{b}$ is the shear of the martensite, and $\mathbf{F}_M$ is the average deformation gradient of the twinned martensite. When the twins are fine enough, $\mathbf{F}_M$ satisfies

$$\mathbf{F}_M = \mathbf{R}_h[f\mathbf{R}_{ij}\mathbf{U}_i + (1-f)\mathbf{U}_i] \qquad [15]$$

where $\mathbf{U}_i$ and $\mathbf{U}_j$ are the two lattice correspondence variants in the twin, and $(1-f)$ and f are their volume fractions. The term $\mathbf{R}_h$ is the relative rotation between the twinned martensite and the parent phase. The values of $\mathbf{R}_h$ and f are unknown and will be determined in the following. Upon substituting Eqs. [5] and [15] into Eq. [14], we obtain

$$\mathbf{R}_h[U_i + f\,\mathbf{a} \quad \mathbf{n}] = \mathbf{I} + \mathbf{b} \quad \mathbf{m} \qquad [16]$$

There are six equations in Eq. [16] since there are six possible pairs of (**a**, **n**). Following the procedure of solving Eq. [5], we form matrix $\mathbf{C}(f)$ as

$$\mathbf{C}(f) = (\mathbf{U}_i + f\mathbf{n} \quad \mathbf{a})(\mathbf{U}_i + f\mathbf{a} \quad \mathbf{n}) \qquad [17]$$

Again, the sufficient and necessary condition for Eq. [16] having solutions is that $\mathbf{C}(f)$ has ordered eigenvalues of $\lambda_1 \leq \lambda_2 = 1 \leq \lambda_3$. So, the volume fraction f can be obtained by

$$\det(\mathbf{C}(f) - \mathbf{I}) = 0 \qquad [18]$$

where det $(\cdot)$ is the determinant of a matrix. Substituting the preceding six possible twins into Eqs. [17] and [18], the solutions of f, ordered eigenvalues of $\lambda_1 \leq \lambda_2 = 1 \leq \lambda_3$, and the corresponding eigenvectors $\mathbf{e}_1$, $\mathbf{e}_2$, and $\mathbf{e}_3$ are obtained. And the solutions of **b** and **m** in Eq. [16] are

$$\mathbf{b} = \rho\left(\sqrt{\frac{\lambda_3(\lambda_2 - \lambda_1)}{\lambda_3 - \lambda_1}}\,\mathbf{e}_1 + \kappa\sqrt{\frac{\lambda_1(\lambda_3 - \lambda_2)}{\lambda_3 - \lambda_1}}\,\mathbf{e}_3\right) \qquad [19]$$

$$\mathbf{m} = \rho^{-1}\left(\frac{\sqrt{\lambda_3} - \sqrt{\lambda_1}}{\sqrt{\lambda_3 - \lambda_1}}\right)(-\sqrt{\lambda_2 - \lambda_1}\mathbf{e}_1 + \kappa\sqrt{\lambda_3 - \lambda_2}\mathbf{e}_3) \qquad [20]$$

The definitions of the parameters in Eqs. [19] and [20] are similar to those in Eqs. [10] and [11]. Only that ρ is used to make **m** as a unit normal vector. Equations [19] and [20] also represent two sets of (**b**, **m**) because of $\kappa = \pm 1$.

Proposition 5 of Ball and James[12] gives $\det(\mathbf{C}(f) - \mathbf{I}) = \det(\mathbf{C}(1 - f) - \mathbf{I})$; i.e., if f is a solution of Eq. [18], $1 - f$ is also a solution of Eq. [18]. Generally, matrices $\mathbf{C}(f)$ and $\mathbf{C}(1 - f)$ have different eigenvalues and eigenvectors. Therefore, for each twin (corresponding to a pair of (**a**, **n**)), we get two solutions of f from Eq. [18]. Then, for each volume fraction f, two sets of (**b**, **m**) are obtained from Eqs. [19] and [20]. Therefore, the total number of habit plane variants are $6 \times 2 \times 2 = 24$.

Once the habit plane orientations and the transformation strains are determined, it is possible to establish the transformation strain as

$$\varepsilon^{CV} = \frac{1}{2}(\mathbf{F}_M^T \cdot \mathbf{F}_M - \mathbf{I}) = \frac{1}{2}[\mathbf{b} \quad \mathbf{m} + \mathbf{m} \quad \mathbf{b} + (\mathbf{b} \cdot \mathbf{b})\mathbf{m} \quad \mathbf{m}] \qquad [21]$$

In Eq. [21], **b** is not a unit vector and includes the shear magnitude. The magnitude of the transformation is determined as $|\mathbf{b}| = 0.1823$. One of the variants has a twin volume fraction f and the other has a twin volume fraction $(1 - f)$ in the CVP. The values of all the transformation vectors are determined as $\mathbf{n} = \{\bar{1},1,0\}$, $\mathbf{a} = \langle 0.4151, 0.3155, 0\rangle$, and $\eta_1 = \langle 1,1,0\rangle$, where **n** is the twinning plane normal and **a** is the twinning shear direction. The habit planes and directions are $\mathbf{m} = \{0.744, 0.1289, -0.6552\}$, $\mathbf{b} = \langle 0.1241, -0.02577, 0.1310\rangle$, where **m** is the habit plane normal and **b** is the transformation shear of the martensite. The twin plane $\mathbf{K}_1$ is the same as **n**, while the twinning direction η_1 is equal to $\mathbf{U} \cdot \mathbf{a}$, where **U** is the symmetric part of the deformation gradient matrix. There are two solutions for the volume fraction of the variants in a CVP (f is 0.351 or 0.649). The CVP includes two twin-related variants. The total number of CVPs for the austenite to martensite transformation is 24 for this class of alloys.

The detwinning strain (conversion of the one volume fraction variant to the other one within the CVP) can be determined as follows. From Eq. [15], variant $\mathbf{U}_j$ converses to $\mathbf{U}_i$ if volume fraction $f < 0.5$, and the deformation after detwinning is (by setting $f = 0$)

$$\mathbf{F}_M^{dt} = \mathbf{R}_h\mathbf{U}_i \qquad [22]$$

If the volume fraction f is greater than 0.5, variant $\mathbf{U}_i$ converses to $\mathbf{U}_j$ and the transformation including detwinning is given by setting $f = 1$ as

$$\mathbf{F}_M^{dt} = \mathbf{R}_h\mathbf{R}_{ij}\mathbf{U}_j = \mathbf{R}_h \cdot (\mathbf{U}_i + \mathbf{a} \quad \mathbf{n}) \qquad [23]$$

Once the $\mathbf{F}_M^{dt}$ is known, the transformation strain (including CVP formation and detwinning) can be determined similar to Eq. [21] with F_M replaced by F_M^{dt}.

$$\varepsilon^{dt} = \frac{1}{2}(\mathbf{F}_M^{dtT} \cdot \mathbf{F}_M^{dt} - \mathbf{I}) \qquad [24]$$

The total recoverable strain is the sum of the CVP formation strain and the detwinning strain (Eq. [24]). The summary of the theoretical calculations are given in Figures 3(a) through (d). The results are given as contour plots in these figures. We include the transformation strains associated with CVP formation and also for combined CVP formation and detwinning. The effect of detwinning is to increase the overall transformation strains in both tension and compression in most crystal orientations. We also note that the detwinning strains in compression far exceed those observed in tension loadings for most orientations. The highest transformation strains are near the [001] pole for both tension and compression. These findings show that the transformation strains in Fe-based alloys can potentially be high and comparable to NiTi alloys.

IV. TENSION-COMPRESSION EXPERIMENTS

To understand the stress-strain response of transforming FeNiCoTi materials, we consider the schematic shown in Figure 4. Upon deformation in the elastic regime, the material deforms with an austenite elastic modulus of E_A; the austenite to martensite transformation starts extremely early in the stress-strain curve (based on the resistivity measurements to be reported later in this article). The austenite to martensite transformation proceeds over an ascending stress-strain curve in both single and polycrystalline alloys. The austenitic matrix slips as the strain levels are increased further. Upon unloading, the elastic modulus corresponds to that of a dual-phase structure, including both the austenite and the martensite. Based on our measurements of the unloading modulus, we find that the elastic modulus of the dual-phase structure (hence, the martensite) is lower than the austenite. Two types of recoverable strains can be observed: pseudoelasticity and shape memory. The pseudoelasticity portion of the recoverable strain is the portion that reverts back to austenite upon unloading, while the shape memory part corresponds to the strain that recovers upon heating the

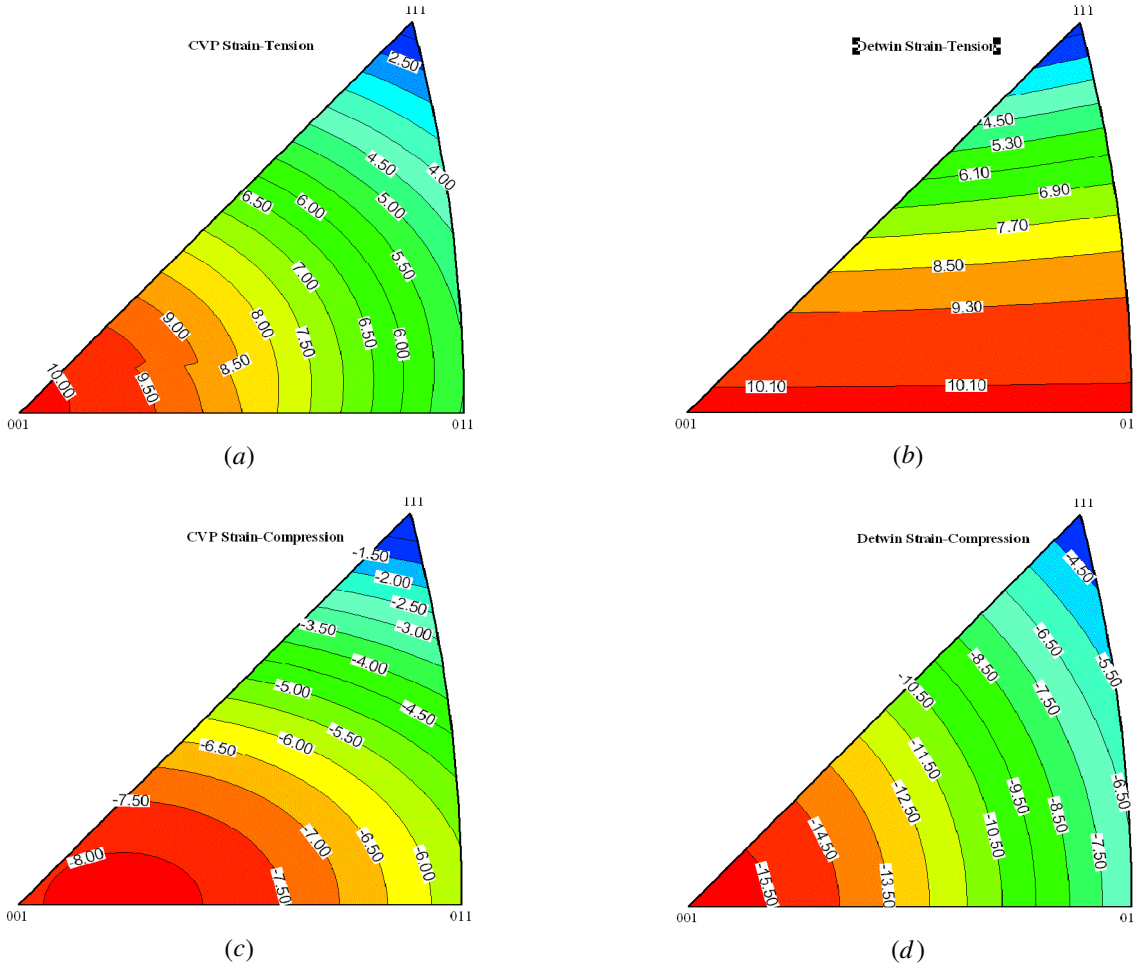

Fig. 3—(*a*) Transformation strain contours for FeNiCoTi alloy in tension. (*b*) Transformation strain contours for FeNiCoTi alloy in tension after detwinning of the CVP. (*c*) Transformation strain contours for FeNiCoTi alloy in compression. (*d*) Transformation strain contours for FeNiCoTi alloy in compression after detwinning.

sample to above austenite finish temperatures. The pseudoelasticity contribution is rather small in the case of Fe-based shape memory alloys.

The experiments were conducted at room temperature under strain control. The specimen cross section for compression was square with 4-mm width and the height of the specimen was 8-mm. The tension specimens were dog-bone shaped with a gage length of 8-mm, width of 3-mm, and thickness of 1-mm. For accurate measurement of strains, a miniature extensometer was used. The temperature was monitored during testing to ensure that the temperature rise due to transformation is less than 1 °C.

The stress-strain curves in tension are shown in Figures 5(a) and (b) for the [123] and polycrystalline cases, respectively. The specimens were deformed to strain levels near 1.5 pct in all cases. The strain variation upon heating and cooling at zero load is indicated by the line with an arrow. We note that the strength level in the polycrystalline case is substantially higher than that in the [123] case. Figures 6(a) and (b) depict the microstructure of the polycrystalline specimen with the presence of martensite upon unloading to zero load. Then, upon heating above the austenite finish temperature, the martensites disappear, as shown in Figure 6(b). Similar observations were made for the [123] single crystals. The martensite variants are in Figure 7(a). The variants transform to austenite upon heating above the austenite finish temperature, as shown in Figure 7(b).

The results for the compression case are given in Figures 8(a) and (b) for the [123] and polycrystalline cases, respectively. Similar to the tensile case, the FeNiCoTi in single-crystal and polycrystalline forms exhibits shape memory behavior in compression. We note that the stress-strain responses in Figures 5(b) and 8(b) are different.

We now check whether the recovery in transformation strains can be substantiated with the return of the electrical resistance to its reference level after deformation and heating. By using an *in-situ* electrical resistance measurement technique, we monitored the changes during a tensile deformation experiment.

The experimental results for tensile deformation at 100 °C are given in Figure 9. The transformation-induced resistivity change $\left[\frac{\Delta R}{R_0}\right]_{\text{trans}}$ is shown on the right vertical axis. The reference resistivity is measured at 100 °C as 3.2 mΩ. The specimen is deformed at 100 °C and then unloaded to zero load. The changes in resistance are negative and nearly 10 pct when the applied strain reaches near 1.5 pct. Our later results will confirm that, upon austenite to martensite transformation, the electrical resistance decreases and *vice versa*

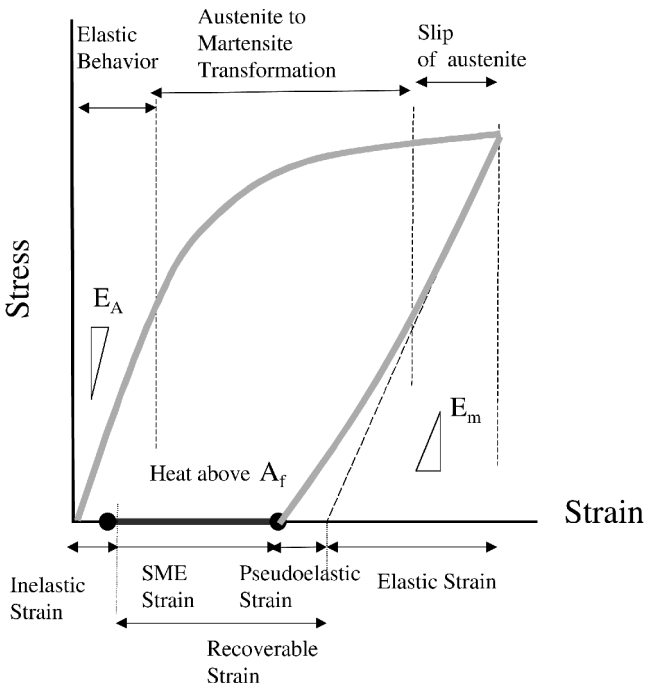

Fig. 4—Schematic of stress-strain response of Fe-based transforming alloys at constant temperatures.

upon reverse transformation. The resistance change is in the reverse direction upon unloading. When the specimen is heated to above austenite finish temperature, the resistance (shown as a dashed line) rapidly approaches the reference level of electrical resistance.

V. TEMPERATURE CYCLING UNDER CONSTANT STRESS

To gain further insight into results, the specimens were subjected to thermal cycling conditions. The experiments were conducted under stress control and axial deformation was monitored during the experiments. A schematic of strain temperature response of a single crystal is shown in Figure 10(a). When the temperature is above the austenite finish temperature, $T > A_f$, the material is in the austenitic (fcc) phase. The transformation behavior is studied under constant stress. The martensite that is formed at the martensite start temperature is internally twinned. The martensite detwins (one twin variant grows at the expense of the other) as the temperature is lowered further. Ultimately, a single crystal of martensite is formed. Near the martensite finish temperature, M_f, the austenite is entirely converted to martensite. Depending on the stress level, slip can occur in the austenitic domains first and can spread to martensitic regions. We provided evidence of slip deformation with transmission electron microscopy earlier in this article.

In the experiments, the temperature was cycled between −130 °C to as high as 220 °C. The duration of heating and cooling was approximately 60 minutes per cycle to minimize transient effects and thermal gradients. The experimental results are summarized in Figure 10(b) for two stress levels. Other stress levels were also considered but not reported here. If the stress level is increased, the transformation strains increase, and at the same time, the martensite start temperature shifts. The martensite start temperature is approximately

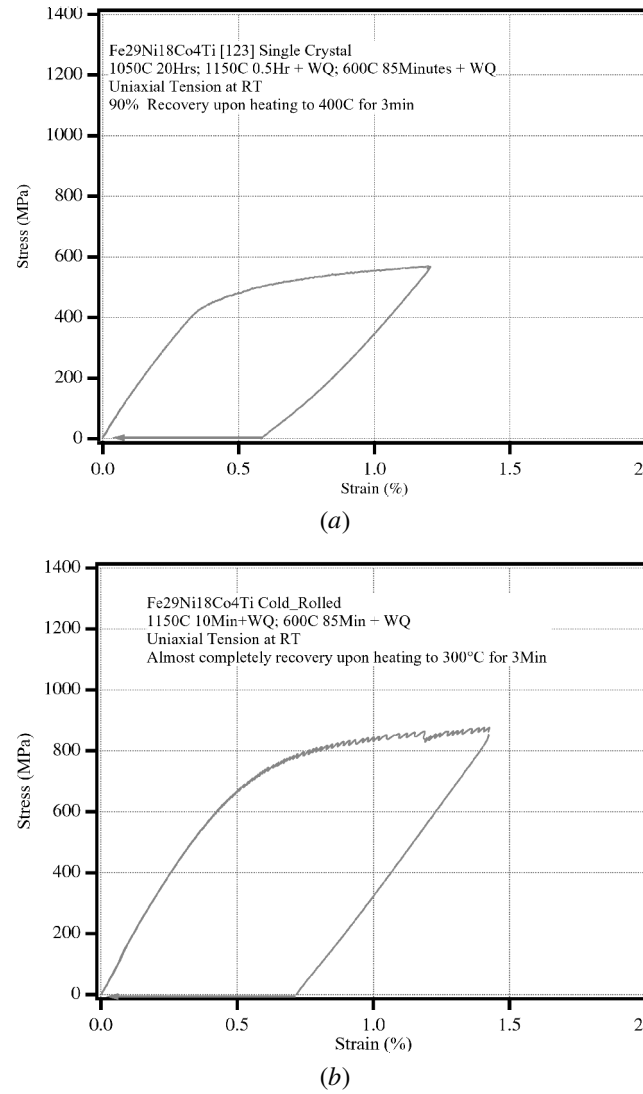

Fig. 5—Stress-strain response of FeNiCoTi in tension at room temperature. After unloading, the specimen is heated to 300 °C or 400 °C at zero load and the recoverable strains are denoted with an arrow: (*a*) single crystal with [123] orientation and (*b*) polycrystalline specimen.

−80 °C, while the austenite start temperature is near 0 °C for the 400 MPa case. It is more difficult to identify the martensite finish and austenite finish temperatures because the tails of the curves do not perfectly flatten. With different aging treatments, these transformation temperatures are expected to vary. We have conducted *in-situ* optical microscopy during these experiments and observed that the transformation temperature range is much broader than the conventional shape memory alloys. For example, the transformation temperature in this case is nearly 200 °C compared to 80 °C in NiTi alloys.

The resistance change during the transformation is shown in Figure 11. The vertical axis is normalized by the reference level electrical resistance, R_0. The reference resistivity is the room temperature resistivity of 2.98 mΩ. We note that the resistance decreases sharply when the martensite start temperature is reached (consistent with Figure 10(a)). Upon austenite to martensite transformation, the resistance change is approximately −30 pct, which is completely recovered upon heating to the austenite finish temperature. The cooling

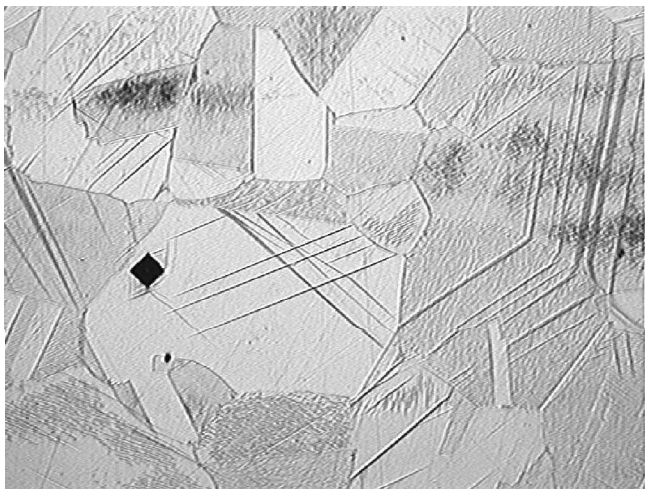

(*a*)

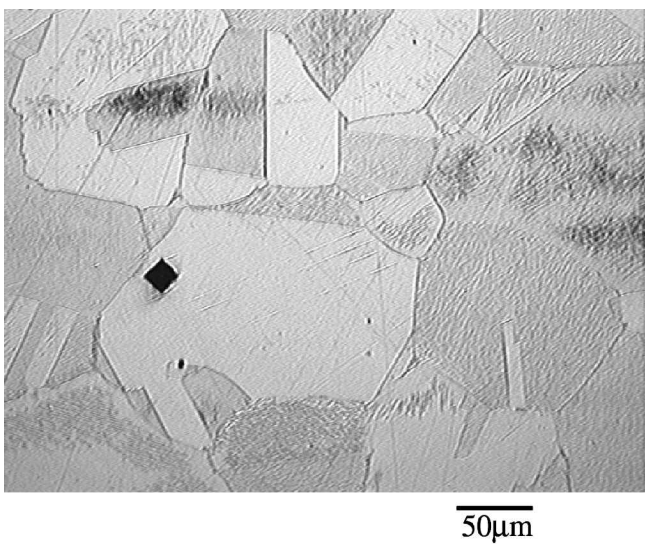

(*b*)

Fig. 6—(*a*) Optimal microscopy image of polycrystalline (cold-rolled) specimen subjected to tension (in the unloaded state) and (*b*) after recovery upon heating to 300 °C for 3 min. Note that an indenter has been placed to ensure that the same location is viewed before and after deformation.

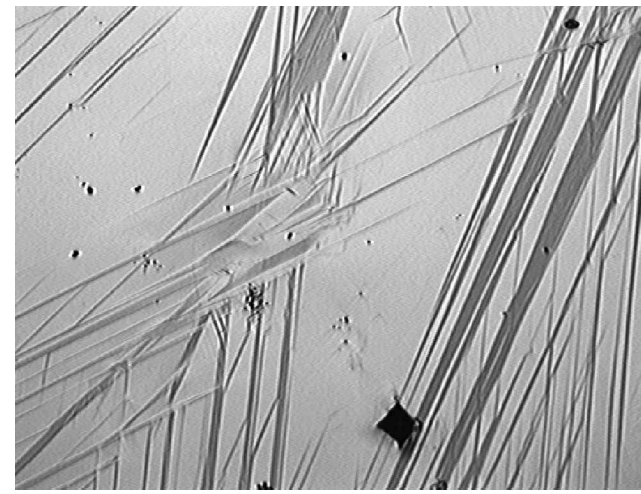

(*a*)

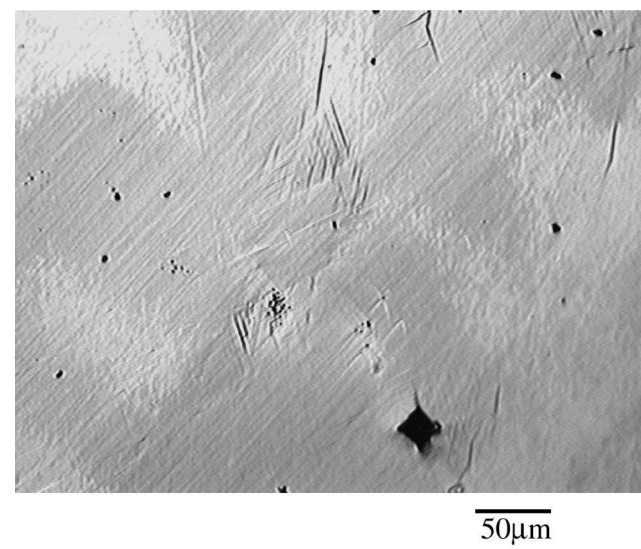

(*b*)

Fig. 7—(*a*) [123] specimen subjected to tension and (*b*) after recovery upon heating to 400 °C for 3 min. The indentation mark is shown in the lower portion of the figures.

and heating portions of the curves are shown with arrows. Optical *in-situ* photographs have been obtained depicting the presence of a high volume fraction of martensite at low temperatures, which are fully recovered upon heating to temperatures near 150 °C. We note that the test conditions between Figure 11 (−30 pct change) and Figure 9 (−10 pct change) are different.

VI. DISCUSSION OF RESULTS

Based on the electrical resistance measurements, the results show that the transformation nucleates during unidirectional deformation at stress levels in the elastic regime (Figure 9). As the martensite volume fraction increases during the ascending portion of the stress-strain curve, the electrical resistance decreases compared to its reference value. The transformation proceeds in a nonhomogenous fashion in the austenite domains, as shown with *in-situ* optical microscopy and postexperimental transmission electron microscopy. Selective transformation is expected to occur near precipitates at locations where the applied shear stresses and the local shear stresses resolved on the most favorably oriented CVP reach a critical value. At strains exceeding 3 pct, the reversibility of the transformation is limited. However, below 3 pct, we observe recovery upon heating above the austenite finish temperature. Apparently, at high strains, two factors play a role. Extensive slip spreads across the austenitic domains, and the martensite structure (although rather strong) is deformed enough where it cannot revert back to the austenite.

The transformation stress and transformation strain have been found to be rather sensitive to the aging treatment. Slight changes in the aging treatment lowered the transformation stress and at the same time lowered slip resistance. It has been found that the resistance to slip is by far the most important criterion to achieve reversible transformation in this class of alloys. The multiplicity of slip systems and the localized slip at grain boundaries (in the polycrystalline

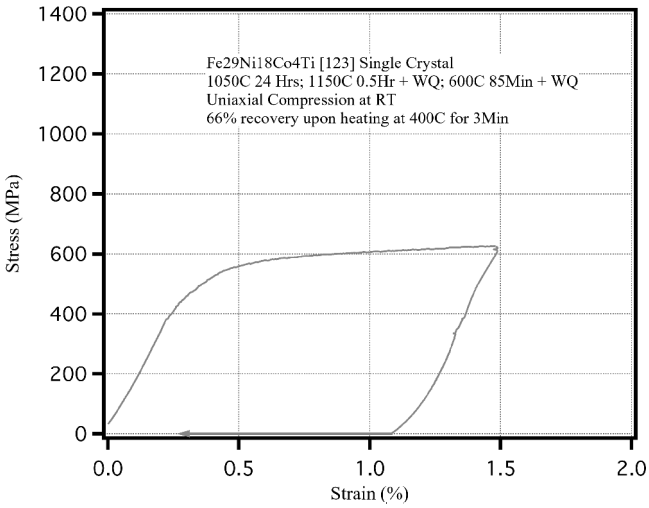

(*a*)

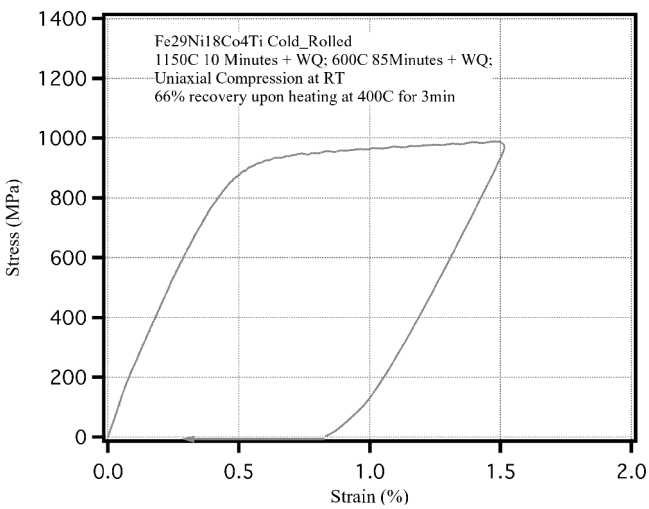

(*b*)

Fig. 8—Stress-strain response of FeNiCoTi in compression at room temperature. After unloading, the specimen is heated to 400 °C at zero load and the recoverable strains are denoted with an arrow: (*a*) single crystal with [123] orientation and (*b*) polycrystalline specimen.

case) in the fcc structure promoted the occurrence of finite local dislocation densities.

The transformation stress at high temperatures (100 °C) is considerably higher compared to results at room temperature (Figure 5(b) and 9 comparison). In the case of NiTi alloys, the M_d temperature (the temperature above which martensite cannot be induced) is nearly 80 °C higher than the martensite start temperature. In the FeNiCoTi alloys, the temperature range over which martensite can be stress induced is as high as 150 °C. The results point to the need to enhance slip resistance at high temperatures as a criterion to maximize the transformation in FeNiCoTi alloys. The deformation temperature relative to the M_d temperature is an important consideration in interpretation of all results in shape memory alloys. Thermomechanical treatments are being explored to increase the strength of the austenite phase, thereby extending the region of transformation.

The experimental results demonstrate that the recoverable (transformation) strains for the FeNiCoTi compositions are lower than those for the NiTi alloys. However, the strength

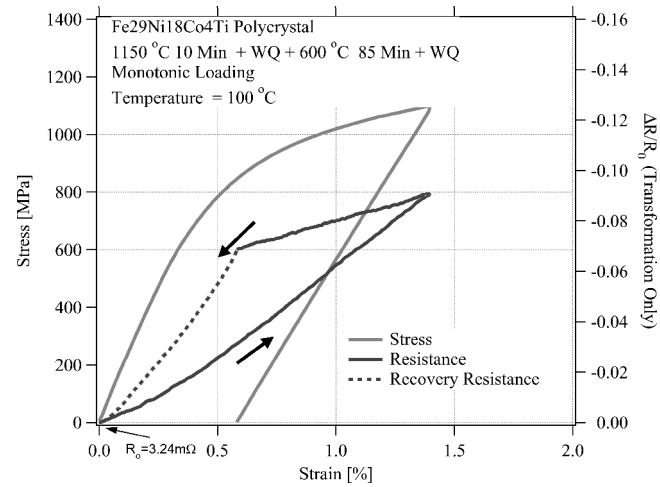

Fig. 9—Stress-strain response and the corresponding changes in resistivity for the polycrystalline material in tension at 100 °C. We note that the resistivity is normalized with respect to the reference level. The dashed line demonstrates recovery upon heating to above the austenite finish temperatures.

(transformation stress) levels in the FeNiCoTi are higher by as much as 500 MPa. In this regard, the behavior of FeNiCoTi is comparable to 51.5 pct NiTi alloys, as recently reported by the authors.[15] In the case of 51.5 pct NiTi alloys, the higher volume fraction of precipitates (>20 pct), which are untransformable, produced lower transformation strains (maximum of 3.7 pct). In the Fe alloys, dislocation generation is responsible for the lower transformation strains compared to the theoretically possible levels. The presence of a high volume fraction of precipitates is also noted for the FeNiCoTi alloys, and the number of variants activated is expected to deviate compared to the phenomenological theory of transformations. The multivariant structure has been observed in the [123] case (Figure 7(a)) despite the single CVP predicted by the theory.

The stress required for stress-induced martensite increases with increasing temperature. This stress to produce stress-induced martensite follows the Clausius–Clapeyron equation, given as

$$\frac{d\sigma}{dT} = \frac{\Delta H}{\varepsilon T}$$

where ΔH is the transformation latent heat, ε is the transformation strain for CVP formation, and T is the temperature. The Clausius–Clapeyron equation can be represented as a shift (increase) in the martensite start temperature with applied stress. Based on the stress-strain responses shown in Figures 5(b) and 9 (deformation at 22 °C and 100 °C), we determined the critical stress for transformation as 660 MPa and 819 MPa (0.1 pct offset); hence, we evaluated the slope of the stress-temperature curve as 1.59 MPa/K. Similarly, the strain-temperature curve given as Figure 10(b) can be used to determine the shift in martensite start temperature with increasing stress. The slope $d\sigma/dM_s$ is determined as 1.6 MPa/K. This agreement between the two slopes has been observed in other shape memory alloys. The major difference between this alloy and the NiTi shape memory alloys is that the slope in NiTi is nearly 5 times higher.

These results have important consequences for the ability of the Fe-based shape memory alloy to exhibit pseudoleastic

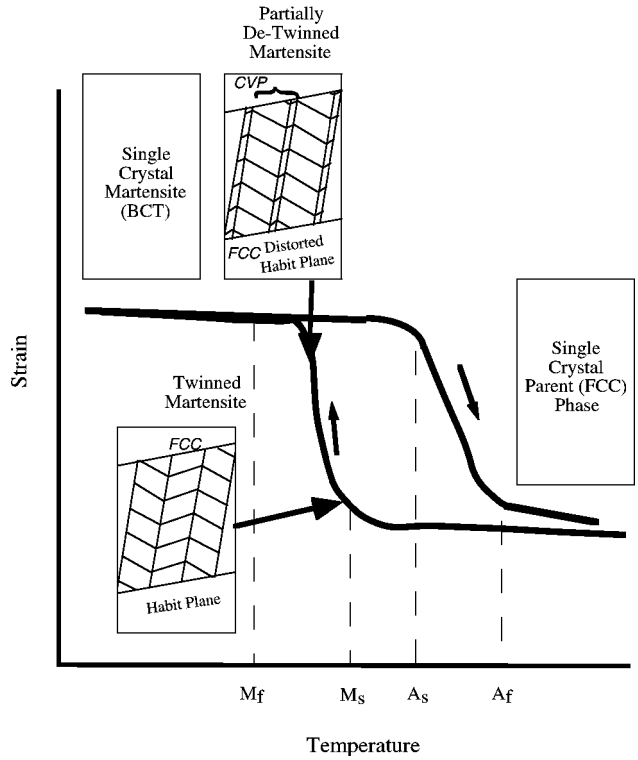

(*a*)

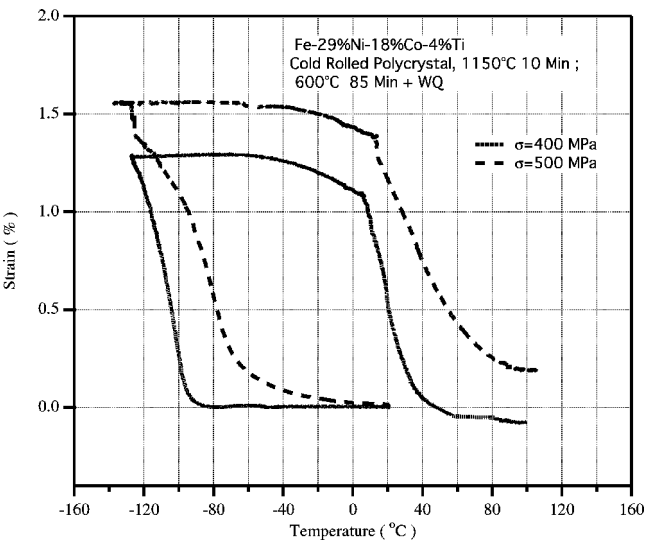

(*b*)

Fig. 10—(*a*) Schematic of strain-temperature behavior of the FeNiCoTi (polycrystalline) alloy showing the martensite start temperature upon cooling and austenite start temperature upon heating. (*b*) Experimental results of strain upon temperature cycling displaying the role of stress on transformation temperatures and the strain levels.

behavior. Previous work on NiTi shape memory alloys noted that pseudoelasticity has occurred at nearly 20 °C to 50 °C above the martensite start temperature. Several criteria must be met, as discussed by Liu and Galvin,[16] to achieve pseudoleasticity: high austenite strength, a low critical stress for transformation, and a small temperature difference between the austenite finish and martensite start points (a narrow hysteresis) promote pseudoelasticity. The Fe-based alloys exhibit a wide thermal hysteresis (Figure 10(b)) and a high

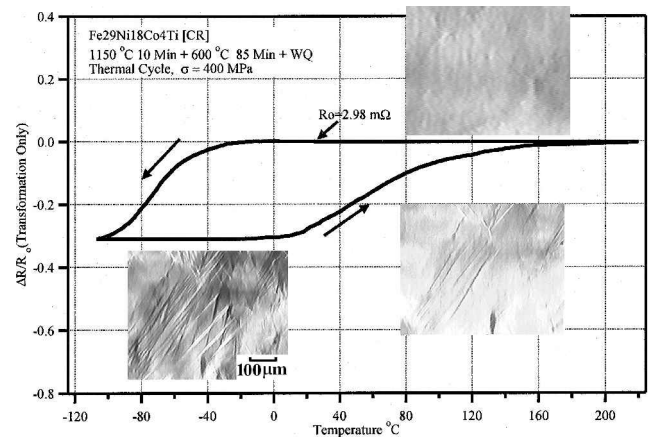

Fig. 11—The change in resistivity (normalized by the resistivity at room temperature) as a function of temperature cycling. The lower picture depicts the martensite at 0 °C. The image on the bottom right shows the partially recovered martensite at temperatures near 120 °C, and the upper picture represents the 100 pct austenite at room temperature after all the martensite has reverted to austenite. Photographs are taken *in-situ* during the testing.

critical stress for transformation. With suitable heat treatments and compositional variations, it would be possible to achieve optimum conditions in the Fe-based shape memory alloys.

The present results indicate that if we can tailor the texture of polycrystals to a [001] type, then we can develop superior compressive actuators. The [001] orientation has the highest transformation strains among all orientations, as shown in Figure 3. However, the [001] orientation is conducive to slip deformation based on the Schmid factor calculations (=0.41) for the austenitic (parent) fcc lattice. The mechanical twinning can partially explain the lower recoverability levels in compression compared to tension in our experiments. Therefore, any treatments that increase the austenite flow stress, such as through increase in volume fraction of precipitates, or texture in the case of polycrystals would increase the transformation strain.

VII. CONCLUSIONS

1. The results show that the FeNiCoTi alloy exhibits high strength and high pct SME (shape memory effect). Tension-compression asymmetry of yield stresses was clearly demonstrated for both the single-crystal [123] and polycrystalline samples. Theoretical calculations of transformation strains point out that this class of alloys has a strong potential for shape memory applications, especially with further optimization of composition and heat treatments.
2. Electrical resistance variations as high as 30 pct (with respect to reference levels) were measured corresponding to austenite to martensite transformation. Upon reverse transformation from martensite to austenite, the electrical resistance returned to its reference level. These results confirm that the transformation is reversible in the FeNiCoTi alloys.
3. Extensive *in-situ* optical microscopy and postexperimental transmission electron microscopy were conducted on both the single-crystal and polycrystalline samples. The optical microscopy demonstrated the reversibility of the

martensite variants, while the transmission electron microscopy results revealed the presence of slip, at the interface of austenite/martensite domains, in addition to restricted slip in austenite domains. The slip deformation limits the full recoverability of transformation in this class of alloys.

4. The theoretical results demonstrate that, in applications where high recoverable strains are required, it is recommended to texture the polycrystals in the ⟨001⟩ direction. The theoretical transformation strains are as high as 10 to 15 pct depending on the crystal orientation, making these materials extremely attractive in shape memory applications.

ACKNOWLEDGMENTS

This work was supported by the Air Force Office of Scientific Research, under Grant No. F49620-01-1-0136.

REFERENCES

1. H. Funakubo: *Shape Memory Alloys*, Gordon and Breach Science Publishers, New York, NY, 1989.
2. H. Sehitoglu, I. Karaman, R. Anderson, X. Zhang, K. Gall, H.J. Maier, and Y. Chumlyakov: *Acta Mater.*, 2000, vol. 48 (13), pp. 3311-26.
3. H. Sehitoglu, I. Karaman, X. Zhang, A. Viswanath, Y. Chumlyakov, and H.J. Maier: *Acta Mater.*, 2001, vol. 49 (17), pp. 3621-34.
4. T. Maki: in *Shape Memory Materials*, K. Otsuka and C.M. Wayman, eds., Cambridge University Press, Cambridge, United Kingdom, 1998, ch. 5.
5. V.V. Kokorin, L.P. Gunko, and O.M. Shevchenko: *Scripta Mater.*, 1993, vol. 28, pp. 35-40.
6. L.P. Gunko, V.V. Kokorin, and O.M. Shevchenko: *Phys. Met. Metall.*, 1991, vol. 72 (4), pp. 209-13.
7. E. Cesari, V.A. Chemenko, V.V. Kokorin, J. Pons, and C. Segui: *Scripta Mater.*, 1999, vol. 40 (3), pp. 341-45.
8. N. Jost, K. Escher, P. Donner, M. Sade, K. Halter, and E. Hombogen: *Wire*, 1990, vol. 40 (6), pp. 639-40; also N. Jost: *Metall.*, 1990, vol. 44 (1), pp. 17-22.
9. H. Kloss: *Z. Metallkd.*, 1996, vol. 3, pp. 175-78.
10. T. Maki: *MRS Int. Meeting Adv. Mater.*, 1989, vol. 9, pp. 415-42.
11. H. Sehitoglu, I. Karaman, X.Y. Zhang, Y. Chumlyakov, and H.J. Maier: *Scripta Mater.*, 2001, vol. 44 (5), pp. 779-84.
12. J.M. Ball and R.D. James: *Arch. Rat. Mech. Anal.*, 1987, vol. 100, pp. 13-52.
13. V.V. Kokorin, Y.I. Samsonov, L.F. Khshanovskiy, V.A. Chemenko, and O.M. Shevchenko: *Phys. Met. Metall.*, 1991, vol. 71 (2), pp. 141-46.
14. L.M. Schetky: in *Displacive Transformations and Their Applications in Materials Engineering*, K. Inoue, K. Mukherjee, K. Otsuka, and H. Chen, eds., TMS, Warrendale, PA, 1998, pp. 149-56.
15. H. Sehitoglu, J. Jun, X. Zhang, I. Karaman, Y. Chumlyakov, H.J. Maier, and K. Gall: *Acta Mater.*, 2001, vol. 49 (17), pp. 3609-20.
16. Y. Liu and S.P. Galvin: *Acta Metall.*, 1997, vol. 45 (11), pp. 4431-39.